

Quantum Limits in Scanning Transmission Electron Microscopy

Christian Dwyer^{1,2,*} and David M. Paganin^{3,†}

¹*Electron Imaging and Spectroscopy Tools, PO Box 506, Sans Souci, NSW 2219, Australia,*

²*Physics, School of Science, RMIT University, Melbourne, Victoria 3001, Australia*

³*School of Physics and Astronomy, Monash University, Clayton, Victoria 3800, Australia*

We analyze the quantum limits of four-dimensional scanning transmission electron microscopy (4D-STEM). In estimating the moduli and phases of the Fourier coefficients of the sample's electrostatic potential, we find that 4D-STEM does not permit the quantum limit of precision. In particular, 4D-STEM can attain about half of the available quantum Fisher information. Preclusion of the quantum limit is the result of detection in the diffraction plane, and thus applies to all 4D-STEM techniques. Near-optimum information transfer is achieved by a delocalized speckled probe. We compare with Zernike phase-contrast imaging, which can attain the quantum limit for all spatial frequencies admitted by the optical system, though at lower spatial resolution. Our conclusions also apply to analogous imaging techniques employing other forms of coherent scalar radiation.

Transmission electron microscopy (TEM) has been revolutionized in recent decades by the advent of new classes of pixellated electron detectors having dramatically improved speeds and sensitivities that approach the shot-noise limit. The resulting capacity for “low dose” imaging enables detailed information on radiation-sensitive materials, such as biological, two-dimensional, polymeric, zeolitic, and covalent- and metal-organic-framework materials. The primary concern for any low dose technique is the dose efficiency: Given a “radiation budget” commensurate with preserving the material's atomic structure, what is the ultimate accuracy that can be achieved in measuring the material's properties of interest? Quantum estimation theory can enable answers to such questions, at least within the context of idealized descriptions of the experiments. Despite its idealizations, the formalism can offer significant insight into the limitations of a given technique, and ultimately provide reasons why certain techniques are more dose efficient than others.

Here, we apply the formalism to analyze and optimize the dose efficiency of scanning transmission electron microscopy (STEM) [1]. In STEM, images are generated indirectly by scanning an electron beam across an electron-transparent sample and detecting the scattering in momentum space. Importantly, the spatial resolution so obtained can exceed that of direct image formation. Owing to the improved electron detectors mentioned above, recent years have witnessed a surge in the application of 4D-STEM techniques [2], which use a pixellated detector to capture the diffracted intensity distribution for each beam position (producing a four-dimensional dataset). 4D-STEM can offer significant advantages, including sensitivity to both light and heavy elements within materials, and superb spatial resolution.

Our quantum estimation theory-based analysis reveals that 4D-STEM techniques can attain about half of the available quantum Fisher information, meaning that, for a given level of precision, they require about twice the minimum electron dose permitted by quantum mechanics. Preclusion of the quantum limit is a conse-

quence of detection in the diffraction plane, and it applies to all 4D-STEM techniques, including bright-field, dark-field, differential-phase-contrast [3], center-of-mass [4], matched-illumination [5], symmetry-based [6] and ptychographic [7] imaging. For an arbitrary spatial frequency, near-optimum information transfer is achieved by a delocalized speckled probe.

We compare the dose efficiency with phase-contrast TEM, the standard imaging modality for biological materials and whose collection efficiency is similar to 4D-STEM. Under the Zernike phase condition, phase-contrast TEM provides the greatest sensitivity, in that it enables the quantum limit for all spatial frequencies admitted by the optics. While 4D-STEM generally cannot attain the quantum limit, it yields information on spatial frequencies well beyond those accessible by phase-contrast TEM (for equivalent aberration control).

Background.—Consider the STEM and TEM setups in Fig. 1, where beams of ~ 100 keV electrons pass through an electron-transparent sample. In STEM, a focused beam is scanned, a pixellated detector captures the diffracted intensity for each beam position, and the resulting dataset is processed to form an image. In TEM, we assume fixed parallel illumination at normal incidence, and a pixellated detector captures the image directly.

We assume that the experimental goal is to estimate, simultaneously, a set of P real parameters $\lambda_1, \dots, \lambda_P$, namely, the moduli and phases of the Fourier coefficients of the sample's (projected) electrostatic potential \hat{V} . For materials structure determination, the phases of the Fourier coefficients are usually of particular importance, though we shall mostly treat the moduli and phases on equal footing. We assume that all other parameters, such as those characterizing the optics, are already known with sufficient accuracy.

Quantum and classical Fisher information.—The quantum Fisher information matrix (QFIM), a $P \times P$ matrix denoted J , is a key quantity in quantum estimation theory [8]. J is a quantum analogue of the usual (classical) Fisher information matrix (CFIM), a $P \times P$ matrix

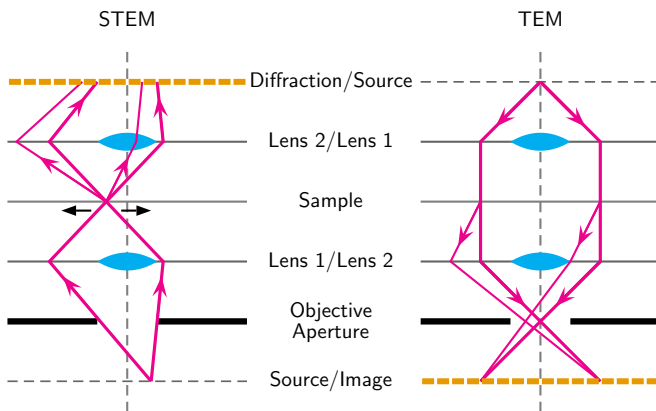


FIG. 1. Electron-optical geometries for 4D-STEM (left) and phase-contrast TEM (right). These reciprocally-related geometries have similar collection efficiencies, and we assume an equivalent degree of aberration control up to the field angles admitted by the objective aperture.

denoted I . In the regime of asymptotic statistics, I and J are related to the attainable variance in the estimation of a parameter λ_μ via the chain of inequalities [9]

$$\text{var}[\lambda_\mu] \geq I_{\mu\mu}^{-1} \geq J_{\mu\mu}^{-1}. \quad (1)$$

$I_{\mu\mu}^{-1}$ is the μ th diagonal element of the inverse matrix I^{-1} , and analogously for $J_{\mu\mu}^{-1}$. Thus, $I_{\mu\mu}^{-1}$ gives the Cramer-Rao lower bound which applies to any (unbiased) estimate of λ_μ , and $J_{\mu\mu}^{-1}$ provides a lower bound for $I_{\mu\mu}^{-1}$. The best (unbiased) estimate obtains *both* equalities, to give $\text{var}[\lambda_\mu] = J_{\mu\mu}^{-1}$. If this is achieved for all parameters $\lambda_1, \dots, \lambda_P$ simultaneously, then the *quantum limit* in the simultaneous estimate of the parameters is achieved. In principle, the first equality can be achieved by using a suitable unbiased estimator for each parameter, such as a maximum likelihood estimator (MLE). However, the second equality can be achieved only under optimum experimental conditions.

For a pure quantum state $|\psi\rangle$, J can be defined as [8]

$$J_{\mu\nu} \equiv 4N \text{Re} \langle \psi_\mu | \hat{Q} | \psi_\nu \rangle, \quad (2)$$

where $|\psi_\mu\rangle \equiv \partial|\psi\rangle/\partial\lambda_\mu$, $\hat{Q} \equiv 1 - |\psi\rangle\langle\psi|$ projects onto the orthogonal complement of $|\psi\rangle$, and N is the number of independent repetitions of the experiment. In our context, N is the number of beam electrons used.

To define the CFIM elements $I_{\mu\nu}$, we assume that the detection of $|\psi\rangle$ is described by a projection-valued measure (PVM) specified by a complete set of projectors $\{|\xi\rangle\langle\xi|\}$. Each projector corresponds to a possible experimental outcome with probability $p(\xi) = |\langle\xi|\psi\rangle|^2$. In this case, $I_{\mu\nu}$ can be written in the form

$$I_{\mu\nu} = 4N \sum_{\xi} \frac{\text{Re}\{\langle\psi_\mu|\xi\rangle\langle\xi|\psi\rangle\} \text{Re}\{\langle\psi|\xi\rangle\langle\xi|\psi_\nu\rangle\}}{\langle\xi|\psi\rangle\langle\psi|\xi\rangle}. \quad (3)$$

It is important to appreciate that, while J involves the state $|\psi\rangle$, it does *not* involve the process of detection. By contrast, I *does* also depend on the specifics of the detection process as represented by the PVM. Loosely, we can think of J and I as the “potential” and “actual” information, respectively. An experiment enables the quantum limit if $I = J$, which is possible if and only if [8, 10]

$$\langle\psi|[\hat{H}_\mu, \hat{H}_\nu]|\psi\rangle = 0 \quad \forall \mu \text{ and } \nu, \quad (4a)$$

$$\langle\psi|\xi\rangle\langle\xi|\hat{Q}|\psi_\mu\rangle \in \mathbb{R} \quad \forall \xi \text{ and } \mu, \quad (4b)$$

where \hat{H}_μ is an Hermitian generator for λ_μ .

In what follows, unless otherwise stated, we adopt the weak phase-object approximation (WPOA) whereby expressions are retained to leading order in the projected potential \hat{V} . The theory is not restricted to this approximation (see Ref. [11] for expressions pertaining to scattering conditions ranging from weak to strong). However, the simplicity of the WPOA allows analytical results which build intuition and pave the way for future work. In the WPOA, condition (4a) is always satisfied.

Our parameters.—In coordinate space, \hat{V} can be written in the form

$$V(x) = \sum_k V(k) e^{2\pi i k \cdot x}, \quad (5)$$

where the Fourier coefficients $V(k)$ obey $V(k) = \bar{V}(-k)$. Our parameters $\{\lambda_\mu\}$ are (a subset of) the Fourier moduli $|V(k_\mu)|$ and phases $\arg V(k_\mu)$, whose spatial frequency k_μ lies in the half space defined by, e.g., $k_x > 0$. The subscript μ on k_μ specifies that it is associated with the parameter set, and when needed we will further specify whether λ_μ means $|V(k_\mu)|$ or $\arg V(k_\mu)$. We will need the derivatives of \hat{V} with respect to each of the parameters, denoted \hat{V}_μ . The derivative of \hat{V} with respect to a modulus $|V(k_\mu)|$ has the Fourier representation

$$V_\mu(k) = \delta_{k, k_\mu} e^{i\phi(k_\mu)} + \delta_{k, -k_\mu} e^{-i\phi(k_\mu)}, \quad (6)$$

where $\phi(k_\mu) \equiv \arg V(k_\mu)$. Similarly, the derivative of \hat{V} with respect to $\arg V(k_\mu)$ has the representation

$$V_\mu(k) = \delta_{k, k_\mu} i V(k_\mu) - \delta_{k, -k_\mu} i \bar{V}(k_\mu). \quad (7)$$

Phase contrast TEM.—We let the incident state $|\psi_0\rangle$ be a plane wave at normal incidence, denoted $|k_0\rangle$ with $k_0 = 0$. We obtain

$$|\psi\rangle = \hat{A}(1 - i\hat{V})|k_0\rangle, \quad (8)$$

where \hat{A} is the (*nonunitary*) operator

$$\hat{A} \equiv \sum_{|k| \leq K} |k\rangle e^{-2\pi i \chi(k)} \langle k|, \quad (9)$$

where $\chi(k)$ is the aberration phase shift, and K is the aperture radius. With the above expressions, we find that the QFIM for TEM is diagonal, with

$$J_{\mu\mu} = 8N |V_\mu(k_\mu)|^2, \quad |k_\mu| \leq K. \quad (10)$$

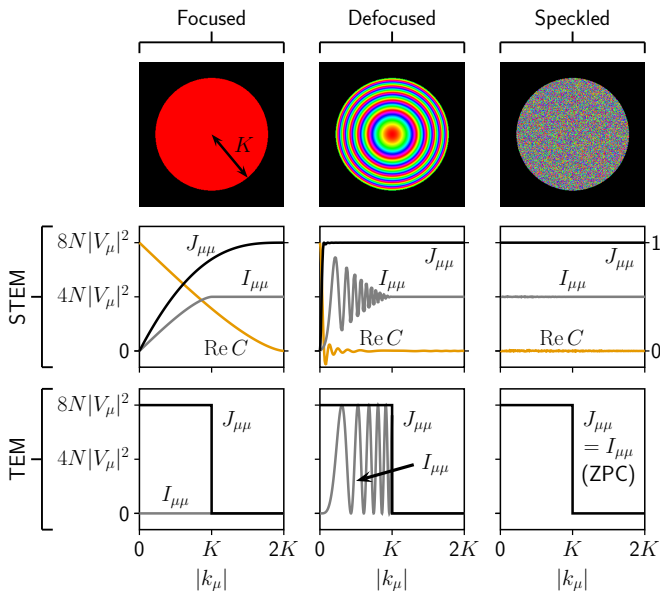


FIG. 2. Quantum $J_{\mu\mu}$ and classical $I_{\mu\mu}$ Fisher information from 4D-STEM and phase-contrast TEM for three different aberration conditions. For each condition, the image shows an RGB plot of the aberration phase shift within the objective aperture, and the graphs show $J_{\mu\mu}$ and $I_{\mu\mu}$ for spatial frequencies up to $2K$. The lower-right graph shows TEM results for the Zernike phase condition (ZPC). For STEM, the real part of the autocorrelation C is also shown (refer to right axis). The value of each curve at $|k_\mu| = 2K$ persists at higher spatial frequencies. A 100 keV beam energy, 20 mrad aperture semi-angle, and -100 nm defocus are assumed (the latter value was chosen to be illustrative rather than optimum).

Here $J_{\mu\mu}$ is independent of the aberrations, and the corresponding quantum limits of precision in the moduli and phases are $\text{var}[|V(k_\mu)|] = 1/8N$ and $\text{var}[\arg V(k_\mu)] = 1/8N|V(k_\mu)|^2$, respectively. The latter variances obey a type of number-phase uncertainty [12].

To determine whether the TEM setup (Fig. 1) permits the quantum limit, we adopt for the PVM the complete set of projectors onto coordinate space $\{\frac{1}{M}|x\rangle\langle x|\}$ (M is the number of points in the discretization of coordinate space). Alternatively to considering (4b), we can calculate the CFIM for TEM directly, which, for $|k_\mu| \leq K$, is

$$I_{\mu\mu} = 4N|V_\mu(k_\mu)|^2 (1 - \cos[2\pi(2\chi(0) - \chi(k_\mu) - \chi(-k_\mu))]). \quad (11)$$

Fig. 2 (bottom row) compares $J_{\mu\mu}$ and $I_{\mu\mu}$ from TEM phase-contrast imaging for different aberration conditions. For perfect focus $\chi(k) = 0$, the image contains no information (as expected). A defocused condition enables the quantum limit for specific spatial frequencies. A Zernike phase condition $\chi(0) = \frac{1}{4}, \chi(k \neq 0) = 0$ enables the quantum limit for all spatial frequencies admitted by the optics [11, 13]. An absolutely key point is that the Zernike condition makes $|\psi\rangle$ real (up to overall phase), so that $|\psi\rangle$ entails optimal interference with greatest possible sensitivity to the parameters of \hat{V} .

4D-STEM.—We regard the 4D-STEM experiment as M independent quantum systems, for which the total quantum state is the tensor product

$$|\Psi\rangle = |\psi(x_1)\rangle \otimes \cdots \otimes |\psi(x_M)\rangle, \quad (12)$$

where $|\psi(x)\rangle$ is a scattered state for which the incident beam was positioned at x in the sample plane. We then use the fact that J (and I) is additive with respect to independent systems [14]. We also introduce the standard notation for the STEM probe wave function $\langle k|\psi_0(x)\rangle = \psi_0(k)e^{-2\pi i k \cdot x}$, where

$$\psi_0(k) = \begin{cases} |\psi_0(k)|e^{-2\pi i \chi(k)} & |k| \leq K, \\ 0 & \text{otherwise.} \end{cases} \quad (13)$$

The QFIM for STEM is found to be diagonal, with

$$J_{\mu\mu} = 8N|V_\mu(k_\mu)|^2(1 - |C(k_\mu)|^2), \quad (14)$$

where $C(k_\mu) = \sum_k \psi_0(k)\bar{\psi}_0(k+k_\mu)$ is an autocorrelation with $C(0) = 1$, and the spatial frequency k_μ is *unrestricted*. Moreover, (14) *does* depend on the aberrations through $C(k_\mu)$. Maximum quantum Fisher information is obtained when $|C(k_\mu)| = 0$ (see discussion).

Notwithstanding the above remarks, 4D-STEM does not enable the quantum limit for any spatial frequency. To see why, we adopt for the PVM the complete set of projectors onto Fourier space $\{|k\rangle\langle k|\}$, and we consider the reality condition (4b).

For wave vectors k in the bright field, assuming that $|C(k_\mu)| \approx 0$ (see above), (4b) becomes

$$-i\bar{\psi}_0(k)\psi_0(k-k_\mu)V_\mu(k_\mu)e^{+2\pi i k_\mu \cdot x} + (+k_\mu \rightarrow -k_\mu) \in \mathbb{R} \quad \forall x, |k| \leq K \text{ and } k_\mu, \quad (15)$$

where the notation in parentheses implies the preceding term with $+k_\mu$ replaced by $-k_\mu$. If $|k-k_\mu| \leq K$ and $|k+k_\mu| \leq K$ (the “tunable region,” see Fig. 3), then the two terms in (15) can combine to become real if the aberrations are such that $2\chi(k) - \chi(k-k_\mu) - \chi(k+k_\mu) = n + \frac{1}{2}$ for some integer n . On the other hand, if only $|k-k_\mu| \leq K$ or $|k+k_\mu| \leq K$ (the “untunable region,” see Fig. 3), then, due to the phase factor involving x , the relevant term will be real only for “half” (loosely speaking, though numerically correct) of the beam positions x , regardless of k_μ or χ . Since the untunable region typically comprises a significant portion of the bright field, condition (15) cannot be satisfied.

For k in the dark field, condition (4b) takes the form

$$\sum_{k'} \bar{\psi}_0(k-k')\bar{V}(k')V_\mu(k_\mu)\psi_0(k-k_\mu)e^{-2\pi i(k'-k_\mu) \cdot x} + (+k_\mu \rightarrow -k_\mu) \in \mathbb{R} \quad \forall x, |k| > K \text{ and } k_\mu, \quad (16)$$

where the notation implies a second summation with $+k_\mu$ replaced by $-k_\mu$. For a given k , only one of the summations can be in effect, which means that we cannot balance terms as before. Also notice that (16) is *nonlinear*

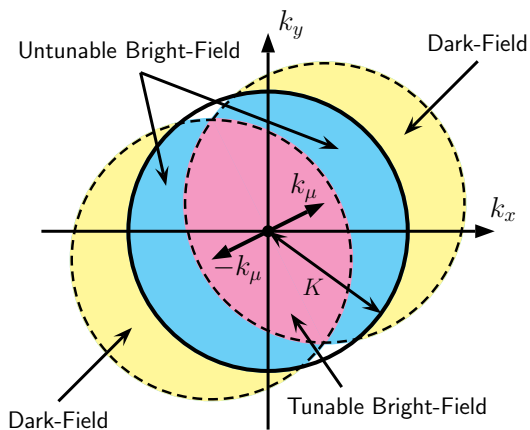


FIG. 3. Bright- and dark-field contributions to the classical Fisher information for a spatial frequency $|k_\mu| \leq K$. Solid circle represents the STEM objective aperture. Dashed circles represent the aperture displaced by $\pm k_\mu$. For $K < |k_\mu| \leq 2K$ (not shown) there is no tunable region. For $|k_\mu| > 2K$ (not shown) there are only dark field contributions.

in \hat{V} , which prevents us from obtaining general results. However, when multiple spatial frequencies k' contribute to the summation, then, owing to the phase factors involving x , there is again a general tendency for the condition to be satisfied for “half” of the beam positions, regardless of k_μ or χ . (There are exceptions to this behavior: If the term $k' = k_\mu$ dominates the summation, as it can when the STEM probe convergence angle is small and there is little overlap of the diffraction discs, then (16) is always satisfied for $\lambda_\mu = |V(k_\mu)|$, i.e., full modulus information, and never satisfied for $\lambda_\mu = \arg V(k_\mu)$, i.e., no phase information. The situation just described is the classic “phase problem.” Notwithstanding such cases, we take as the generic behavior, representative of 4D-STEM, that when multiple spatial frequencies are present.)

Assuming the generic behavior of the dark field, we find that the *complete* CFIM for 4D-STEM is approximately diagonal, with diagonal elements given by

$$I_{\mu\mu} \approx 4N|V_\mu(k_\mu)|^2 \times \left(1 - \sum_k |\psi_0(k - k_\mu)| |\psi_0(k + k_\mu)| \times \cos[2\pi(2\chi(k) - \chi(k - k_\mu) - \chi(k + k_\mu))]\right). \quad (17)$$

Here k_μ is unrestricted. The terms inside the summation are the tunable bright-field contributions, which can range from fully additive (for the previously-stated condition on χ) to fully subtractive (e.g., when $\chi = 0$).

Fig. 2 compares $J_{\mu\mu}$ and $I_{\mu\mu}$ from 4D-STEM for different aberration conditions. Perfect focus results in minimum $J_{\mu\mu}$ (since $|C|$ is maximized) and minimum $I_{\mu\mu}$ (since the tunable contributions are fully subtractive). A defocused condition dramatically improves $J_{\mu\mu}$ and improves $I_{\mu\mu}$ at specific spatial frequencies though not others. For an arbitrary spatial frequency k_μ , a

near-optimum χ is “random” on $[0, 2\pi)$, giving $J_{\mu\mu} \approx 8N|V_\mu(k_\mu)|^2$ and $I_{\mu\mu} \approx \frac{1}{2}J_{\mu\mu}$.

Discussion.—It is a running theme that, for 4D-STEM, the CFIM is approximately half of the QFIM. Thus, 4D-STEM, with its detector positioned in the diffraction plane, precludes the quantum limit in the simultaneous estimation of the Fourier moduli and phases. These conclusions are independent of any data processing of the measured scattering probabilities. Thus, our conclusions apply to any of the current 4D-STEM techniques. In fact, our conclusions apply even more broadly to any similar techniques using other forms of coherent scalar radiation, such as visible light and x-rays.

In 4D-STEM, the aberration-dependence of $J_{\mu\mu}$ can reduce the quantum information for $|k_\mu| \leq 2K$. For k_μ arbitrary, $J_{\mu\mu}$ is near-maximized by a “random” χ , producing a delocalized speckled probe with expected autocorrelation $\langle |C(k_\mu)|^2 \rangle \leq 1/M_K$ (M_K is the number of plane waves inside the aperture) and $I_{\mu\mu} \approx \frac{1}{2}J_{\mu\mu}$. Interestingly, there are several light and x-ray classical-imaging settings where such delocalized speckled illumination is advantageous (e.g., [15]). Low-autocorrelation sequences (e.g., [16]) provide scope for even further optimization of $J_{\mu\mu}$. The χ developed in Ref. [5] is slightly less optimum than random. A defocused χ is most practical using current STEMs, though the information transfer is nonuniform. Note that χ must be effectively known to extract information $I_{\mu\mu}$ from the measured scattering probabilities, and in this sense 4D-STEM is an information encoding-decoding scheme.

The situation regarding the quantum limits of 4D-STEM can be contrasted with that for Zernike phase-contrast TEM, where the latter does enable the quantum limit for all spatial frequencies admitted by the objective aperture. Hence, in principle, for the spatial frequencies that it can access, Zernike phase contrast can match the precision of 4D-STEM using about half of the electron dose. However, the experimental realization of a precise and robust $\pi/2$ phase plate for electrons is highly nontrivial [17], and the Zernike setup is arguably the “more difficult” one in practice. No such phase plate is necessary for 4D-STEM, as it capitalizes on the natural evolution of the scattering to Fourier space. In this sense, preclusion of the quantum limit in 4D-STEM can be viewed as a consequence of the “easier” optical setup.

While it does not enable the quantum limit, 4D-STEM is able to provide information for spatial frequencies well beyond those accessible by direct imaging (for the same degree of aberration control). 4D-STEM also provides more flexibility, since a broad range of image types can be derived. Thus, regarding a choice between the two forms of imaging, based on the present analysis, Zernike phase-contrast TEM should provide greatest sensitivity for resolutions up to about 1 Å, whereas 4D-STEM should be used when larger datasets can be tolerated, flexibility is beneficial, and information is desired at deep-sub-Å

resolutions. We also mention that ptychographical techniques based on 4D-STEM [18] can enable estimates of the sample's electrostatic potential under strong scattering conditions, which is another significant advantage.

Lastly, we remark that the trade off between dose efficiency and spatial resolution in TEM and STEM has been discussed for decades (e.g., [19]). However, what is different about the formalism used here is its generality. This is apparent from the fact that our analyses required no assumptions about how the experimental data is processed. Moreover, the consideration of electron dose is an integral part of the formalism, rather than having to be inferred from additional calculations. Finally, the present formalism readily exhibits the ultimate limits of precision as allowed by the laws of quantum mechanics, and it allows some deeper, significant insights. For example, in the case of Zernike phase-contrast imaging, that the optical setup renders the detected quantum state real is the deeper reason why the quantum limit can be attained. For 4D-STEM, with its indirect image formation via Fourier space, the detected quantum state is inherently complex, and the quantum limit is precluded [20].

The authors acknowledge fruitful discussions with Tim Petersen (Monash University) and Daniel Stroppa (Dectris, Ltd.).

* dwyer@eistools.com

† david.paganin@monash.edu

- [1] P. D. Nellist, in *Springer Handbook of Microscopy*, edited by P. W. Hawkes and J. C. H. Spence (Springer, 2019) Chap. 2.
- [2] C. Ophus, *Microsc. Microanal.* **25**, 563 (2019).
- [3] N. Shibata, S. D. Findlay, Y. Kohno, H. Sawada, Y. Kondo, and Y. Ikuhara, *Nat. Phys.* **8**, 611 (2012).
- [4] K. Müller, F. F. Krause, A. Béché, M. Schowalter, V. Galioit, S. Löffler, J. Verbeeck, J. Zweck, P. Schattschneider, and A. Rosenauer, *Nat. Comm.* **5**, 5653 (2014); E. Yücelen, I. Lazić, and E. G. T. Bosch, *Sci. Rep.* **8**, 2676 (2018).
- [5] C. Ophus, J. Ciston, J. Pierce, T. R. Harvey, J. Chess, B. J. McMorran, C. Czarnik, H. H. Rose, and P. Ercius, *Nat. Comm.* **7**, 10719 (2016).
- [6] M. Krajnak and J. Etheridge, *PNAS* **117**, 27805 (2020).
- [7] P. D. Nellist, B. C. McCallum, and J. M. Rodenburg, *Nature* **374**, 630 (1995); C. T. Putkunz, A. J. D'Alfonso, A. J. Morgan, M. Weyland, C. Dwyer, L. Bourgeois, J. Etheridge, A. Roberts, R. E. Scholten, K. A. Nugent, and L. J. Allen, *Phys. Rev. Lett.* **108**, 173901 (2012); Y. Jiang, Z. Chen, Y. Han, P. Deb, H. Gao, S. Xie, P. Purohit, M. W. Tate, J. Park, S. M. Gruner, V. Elser, and D. A. Muller, *Nature* **559**, 343 (2018); J. Song, C. S. Allen, S. Gao, C. Huang, H. Sawada, X. Pan, J. Warner, P. Wang, and A. I. Kirkland, *Sci. Rep.* **9**, 3919 (2019); M. Schloz, T. C. Pekin, Z. Chen, W. Van den Broek, D. A. Muller, and C. T. Koch, *Opt. Express* **28**, 28306 (2020); Z. Chen, M. Odstrcil, Y. Jiang, Y. Han, M.-H. Chiu, L.-J. Li, and D. A. Muller, *Nat. Comm.* **11**, 2994 (2020); G. Li, H. Zhang, and Y. Han, *ACS Cent. Sci.* **8**, 1579 (2022).
- [8] J. Liu, H. Yuan, X. M. Lu, and X. Wang, *J. Phys. A: Math. Gen.* **53**, 023001 (2020).
- [9] S. L. Braunstein and C. M. Caves, *Phys. Rev. Lett.* **72**, 3439 (1994); S. L. Braunstein, C. M. Caves, and G. J. Milburn, *Annal. Phys.* **247**, 135 (1996).
- [10] K. Matsumoto, *J. Phys. A: Math. Gen.* **35**, 3111 (2002); T. Baumgratz and A. Datta, *Phys. Rev. Lett.* **116**, 030801 (2015); L. Pezze, M. A. Ciampini, N. Spagnolo, P. C. Humphreys, A. Datta, I. A. Walmsley, M. Barbieri, F. Sciarrino, and A. Smerzi, *ibid.* **119**, 130504 (2017); F. Belliard and V. Giovannetti, *New J. Phys.* **23**, 063055 (2021).
- [11] C. Dwyer, *Phys. Rev. Lett.* **130**, 056101 (2023).
- [12] R. Loudon, *The Quantum Theory of Light*, 3rd ed. (Oxford University Press, 2000).
- [13] S. A. Koppell, Y. Israel, A. J. Bowman, B. B. Klopfer, and M. A. Kasevich, *Appl. Phys. Lett.* **120**, 190502 (2022).
- [14] X.-M. Lu, S. Luo, and C. H. Oh, *Phys. Rev. A* **86**, 022342 (2012); G. Tóth and I. Apellaniz, *J. Phys. A: Math. Theor.* **47**, 424006 (2014).
- [15] C. Ventalon and J. Mertz, *Opt. Lett.* **30**, 3350 (2005); E. Mudry, K. Belkebir, J. Girard, J. Savatier, E. Le Moal, C. Nicoletti, M. Allain, and A. Sentenac, *Nat. Photonics* **6**, 312 (2012); A. Gatti, M. Bache, D. Magatti, E. Brambilla, F. Ferri, and L. A. Lugiato, *J. Mod. Opt.* **53**, 739 (2006); S. Bérubon, E. Ziegler, R. Cerbino, and L. Peverini, *Phys. Rev. Lett.* **108**, 158102 (2012); K. S. Morgan, D. M. Paganin, and K. K. W. Siu, *Appl. Phys. Lett.* **100**, 124102 (2012).
- [16] P. Borwein and R. Ferguson, *IEEE Trans. Info. Theory* **51**, 1564 (2005).
- [17] H. Rose, *Ultram.* **110**, 488 (2010); R. M. Glaeser, *Rev. Sci. Instrum.* **84**, 111101 (2013); E. Majorovits, B. Barton, K. Schultheiss, F. Pérez-Willard, D. Gerthsen, and R. R. Schröder, *Ultram.* **107**, 213 (2007); D. Alloyeau, W. K. Hsieh, E. H. Anderson, L. Hilken, G. Benner, X. Meng, F. R. Chen, and C. Kisielowski, *ibid.* **110**, 563 (2010); K. Nagayama and R. Danev, *Phil. Trans. R. Soc. B* **363**, 2153 (2008); R. Danev, B. Buijsse, M. Khoshouei, J. M. Plitzko, and W. Baumeister, *PNAS* **111**, 15635 (2014); H. Müller, J. Jin, R. Danev, J. Spence, H. Padmore, and R. M. Glaeser, *New J. Phys.* **12**, 073011 (2010); O. Schwartz, J. J. Axelrod, S. L. Campbell, C. Turnbaugh, R. M. Glaeser, and H. Müller, *Nat. Meth.* **16**, 1016 (2019).
- [18] A. M. Maiden, M. J. Humphry, and J. M. Rodenburg, *J. Opt. Soc. Am. A* **29**, 1606 (2012); H. G. Brown, Z. Chen, M. Weyland, C. Ophus, J. Ciston, L. J. Allen, and S. D. Findlay, *Phys. Rev. Lett.* **121**, 266102 (2018); Z. Chen, Y. Jiang, Y.-T. Shao, M. E. Holtz, M. Odstrcil, M. Guizar-Sicairos, I. Hanke, S. Ganschow, D. G. Schlom, and D. A. Muller, *Science* **372**, 826 (2021).
- [19] M. G. R. Thomson, *Optik* **39**, 15 (1973); H. Rose, *ibid.* **39**, 416 (1974); **42**, 217 (1975).
- [20] Derivations and auxiliary details are provided in the accompanying supplemental material.

**SUPPLEMENTAL MATERIAL FOR “QUANTUM LIMITS IN SCANNING TRANSMISSION
ELECTRON MICROSCOPY”**

CONVENTIONS

We use the following conventions

$$\mathbb{1} = \sum_k |k\rangle\langle k| = \frac{1}{M} \sum_x |x\rangle\langle x|, \quad (\text{SM.1})$$

where M is the number of points in the discretized 2D coordinate or Fourier space. Also $\langle x|x'\rangle = M\delta_{xx'}$, $\langle k|k'\rangle = \delta_{kk'}$, and $\langle x|k\rangle = e^{2\pi ik \cdot x}$. These produce for the discrete Fourier transform of $\psi(x) = \langle x|\psi\rangle$ and its inverse

$$\psi(k) = \langle k|\psi\rangle = \frac{1}{M} \sum_x \langle k|x\rangle\langle x|\psi\rangle = \frac{1}{M} \sum_x e^{-2\pi ik \cdot x} \psi(x), \quad (\text{SM.2})$$

and

$$\psi(x) = \langle x|\psi\rangle = \sum_k \langle x|k\rangle\langle k|\psi\rangle = \sum_k e^{2\pi ik \cdot x} \psi(k). \quad (\text{SM.3})$$

Normalization of the wave functions is given by

$$1 = \langle \psi|\psi\rangle = \sum_k |\psi(k)|^2 = \frac{1}{M} \sum_x |\psi(x)|^2. \quad (\text{SM.4})$$

The Fourier and coordinate representations of \hat{V} are given by

$$\begin{aligned} \hat{V} &= \sum_{kk'} |k\rangle\langle k|\hat{V}|k'\rangle\langle k'| = \sum_{kk'} |k\rangle V(k-k')\langle k'| \\ &= \frac{1}{M^2} \sum_{xx'} |x\rangle\langle x|\hat{V}|x'\rangle\langle x'| = \frac{1}{M^2} \sum_{xx'} |x\rangle V(x)M\delta_{xx'}\langle x'| = \frac{1}{M} \sum_x |x\rangle V(x)\langle x|. \end{aligned} \quad (\text{SM.5})$$

The discrete Fourier transform and inverse transform of \hat{V} are given by

$$V(k-k') = \langle k|\hat{V}|k'\rangle = \frac{1}{M^2} \sum_{xx'} \langle k|x\rangle\langle x|\hat{V}|x'\rangle\langle x'|k'\rangle = \frac{1}{M} \sum_x e^{-2\pi i(k-k') \cdot x} V(x), \quad (\text{SM.6})$$

and

$$V(x) = \frac{1}{M} \langle x|\hat{V}|x\rangle = \frac{1}{M} \sum_{kk'} \langle x|k+k'\rangle\langle k+k'|\hat{V}|k'\rangle\langle k'|x\rangle = \sum_k e^{2\pi ik \cdot x} V(k). \quad (\text{SM.7})$$

By \hat{V} , we mean the projected electrostatic interaction energy times $1/\hbar v$, where v is the beam electron speed ($V(x)$ is negative for a beam electron interacting with an atom). Analogous expressions hold for \hat{V}_μ .

CALCULATION OF $J_{\mu\nu}$ FOR PHASE-CONTRAST TEM

For phase-contrast TEM, the detected state in the WPOA is given by

$$|\psi\rangle = \hat{A}(1 - i\hat{V})|k_0\rangle. \quad (\text{SM.8})$$

To leading order in \hat{V} , we obtain for the QFIM

$$J_{\mu\nu} = 4N\text{Re} \langle \psi_\mu|\hat{Q}|\psi_\nu\rangle = 4N\text{Re} \langle k_0|\hat{V}_\mu\hat{A}^\dagger(1 - |k_0\rangle\langle k_0|)\hat{A}\hat{V}_\nu|k_0\rangle. \quad (\text{SM.9})$$

Using the expansion

$$\hat{A} = \begin{cases} \sum_k |k\rangle e^{-2\pi i\chi(k)}\langle k|, & |k| \leq K, \\ 0 & \text{otherwise,} \end{cases} \quad (\text{SM.10})$$

we get

$$\begin{aligned}
J_{\mu\nu} &= 4N \left(\sum_{|k| \leq K} \text{Re} \langle k_0 | \hat{V}_\mu | k \rangle \langle k | \hat{V}_\nu | k_0 \rangle - \langle k_0 | \hat{V}_\mu | k_0 \rangle \langle k_0 | \hat{V}_\nu | k_0 \rangle \right) \\
&= 4N \left(\sum_{|k| \leq K} \text{Re} \bar{V}_\mu(k) V_\nu(k) - V_\mu(0) V_\nu(0) \right).
\end{aligned} \tag{SM.11}$$

This vanishes unless $k_\mu = k_\nu$ and $0 < |k_\mu| \leq K$, in which case we obtain

$$J_{\mu\nu} = 4N (\bar{V}_\mu(k_\mu) V_\nu(k_\mu) + V_\mu(k_\mu) \bar{V}_\nu(k_\mu)), \quad 0 < |k_\mu| \leq K. \tag{SM.12}$$

This also vanishes unless μ and ν refer to the same modulus or same phase, that is, $J_{\mu\nu}$ is diagonal. The diagonal elements are given by

$$J_{\mu\mu} = 8N |V_\mu(k_\mu)|^2, \quad 0 < |k_\mu| \leq K, \tag{SM.13}$$

which is Eq. (10) stated in the main text.

CALCULATION OF $I_{\mu\nu}$ FOR PHASE-CONTRAST TEM

We appropriately choose as the PVM the projectors onto coordinate space $\{\frac{1}{M}|x\rangle\langle x|\}$. The CFIM becomes, to leading order in \hat{V} ,

$$I_{\mu\nu} = \frac{4N}{M} \sum_x \frac{\text{Re}\{\langle k_0 | \hat{V}_\mu \hat{A}^\dagger(i) | x \rangle \langle x | \hat{A} | k_0 \rangle\} \text{Re}\{\langle k_0 | \hat{A}^\dagger | x \rangle \langle x | (-i) \hat{A} \hat{V}_\nu | k_0 \rangle\}}{\langle x | \hat{A} | k_0 \rangle \langle k_0 | \hat{A}^\dagger | x \rangle}. \tag{SM.14}$$

Using the expansion of \hat{A} given above, we obtain, for $|k_\nu| \leq K$,

$$\begin{aligned}
\langle k_0 | \hat{A}^\dagger | x \rangle \langle x | \hat{A} \hat{V}_\nu | k_0 \rangle &= e^{2\pi i \chi(0)} \left(e^{2\pi i k_\nu \cdot x - 2\pi i \chi(k_\nu)} V_\nu(k_\nu) + e^{-2\pi i k_\nu \cdot x - 2\pi i \chi(-k_\nu)} \bar{V}_\nu(k_\nu) \right) \\
&= 2|V_\nu(k_\nu)| e^{2\pi i \chi(0) - \pi i \chi(k_\nu) - \pi i \chi(-k_\nu)} \cos[2\pi k_\nu \cdot x - \pi \chi(k_\nu) + \pi \chi(-k_\nu) + \phi_\nu(k_\nu)].
\end{aligned} \tag{SM.15}$$

The relevant real part is

$$\begin{aligned}
\text{Re}\{\langle k_0 | \hat{A}^\dagger | x \rangle \langle x | (-i) \hat{A} \hat{V}_\nu | k_0 \rangle\} &= 2|V_\nu(k_\nu)| \sin[2\pi \chi(0) - \pi \chi(k_\nu) - \pi \chi(-k_\nu)] \\
&\quad \times \cos[2\pi k_\nu \cdot x - \pi \chi(k_\nu) + \pi \chi(-k_\nu) + \phi_\nu(k_\nu)].
\end{aligned} \tag{SM.16}$$

Multiplying by the analogous factor for μ , and summing over x , we obtain that a nonzero result demands $k_\mu = k_\nu$, and then further that $\mu = \nu$, that is, $I_{\mu\nu}$ is diagonal. The diagonal elements can be cast into the form

$$I_{\mu\mu} = 4N |V_\mu(k_\mu)|^2 (1 - \cos[2\pi(2\chi(0) - \chi(k_\mu) - \chi(-k_\mu))]). \tag{SM.17}$$

where $|k_\mu| \leq K$. This form is to be compared with that for 4D-STEM (Eq. (17) in the main text).

CALCULATION OF $J_{\mu\nu}$ FOR 4D-STEM

We regard the STEM experiment as consisting of M independent quantum systems, one system for each position of the electron beam:

$$|\Psi\rangle = |\psi(x_1)\rangle \otimes \cdots \otimes |\psi(x_M)\rangle, \tag{SM.18}$$

where $|\psi(x)\rangle$ is a pure scattered state for which the incident beam was positioned at x in the sample plane, and \otimes denotes a tensor product. Since J (and I) is additive with respect to independent systems, we obtain

$$J_{\mu\nu} = \frac{4N}{M} \sum_x \text{Re} \langle \psi_\mu(x) | \hat{Q}(x) | \psi_\nu(x) \rangle, \tag{SM.19}$$

where $\hat{Q}(x) \equiv 1 - |\psi(x)\langle\psi(x)|$, $|\psi_\mu(x) \equiv \partial|\psi(x)\rangle/\partial\lambda_\mu$, and M is the number of ‘‘pixels’’ in a discretization of the two-dimensional space. With this normalization, N corresponds, as in our analysis of TEM, to the total number of electrons.

Using the POA (not WPOA), we obtain

$$\begin{aligned} J_{\mu\nu} &= \frac{4N}{M} \sum_x \text{Re} \langle \psi_0(x) | e^{+i\hat{V}} \hat{V}_\mu (1 - e^{-i\hat{V}} |\psi_0(x)\rangle \langle \psi_0(x) | e^{+i\hat{V}}) \hat{V}_\nu e^{-i\hat{V}} | \psi_0(x) \rangle \\ &= \frac{4N}{M} \sum_x \text{Re} \langle \psi_0(x) | \hat{V}_\mu (1 - |\psi_0(x)\rangle \langle \psi_0(x) |) \hat{V}_\nu | \psi_0(x) \rangle. \end{aligned} \quad (\text{SM.20})$$

For the first term (containing the identity), we obtain

$$\begin{aligned} &\frac{4N}{M} \text{Re} \sum_{x,k,k',k''} \bar{\psi}_0(k-k') e^{-2\pi i k' \cdot x} \bar{V}_\mu(k') V_\nu(k'') \psi_0(k-k'') e^{2\pi i k'' \cdot x} \\ &= 4N \text{Re} \sum_{k,k'} \bar{\psi}_0(k-k') \bar{V}_\mu(k') V_\nu(k') \psi_0(k-k') \\ &= 4N \sum_{k,k'} |\psi_0(k-k')|^2 \text{Re} \bar{V}_\mu(k') V_\nu(k') \\ &= 4N (\bar{V}_\mu(k_\mu) V_\nu(k_\mu) + V_\mu(k_\mu) \bar{V}_\nu(k_\mu)), \end{aligned} \quad (\text{SM.21})$$

where k_μ is in the half space (defined by, e.g., $k_x > 0$), and we have used $\sum_k |\psi_0(k)|^2 = 1$. From the forms of V_μ given in the main text, μ and ν must both refer to the modulus, or both refer to the phase, otherwise the expression in the last line vanishes. Hence the first term in $J_{\mu\nu}$ equals $8N|V_\mu(k_\mu)|^2 \delta_{\mu\nu}$.

The second term in $J_{\mu\nu}$ is

$$\begin{aligned} &-\frac{4N}{M} \text{Re} \sum_{x,k,k',k'',k'''} \bar{\psi}_0(k) e^{+2\pi i k \cdot x} V_\mu(k-k') \psi_0(k') e^{-2\pi i k' \cdot x} \bar{\psi}_0(k'') e^{+2\pi i k'' \cdot x} V_\nu(k''-k''') \psi_0(k''') e^{-2\pi i k''' \cdot x} \\ &= -4N \text{Re} \sum_{k,k',k''} \bar{\psi}_0(k) V_\mu(k-k') \psi_0(k') \bar{\psi}_0(k'') \bar{V}_\nu(k-k'') \psi_0(k-k'+k'') \\ &= -4N \text{Re} \sum_{k,k',k''} \bar{\psi}_0(k) V_\mu(k') \psi_0(k-k') \bar{\psi}_0(k'') \bar{V}_\nu(k') \psi_0(k'+k'') \\ &= -4N (\bar{V}_\mu(k_\mu) V_\nu(k_\mu) + V_\mu(k_\mu) \bar{V}_\nu(k_\mu)) \left| \sum_k \bar{\psi}_0(k) \psi_0(k-k_\mu) \right|^2, \end{aligned} \quad (\text{SM.22})$$

where, once again, the last line is nonzero only when $\mu = \nu$. Putting the two terms together, we have, for the diagonal elements

$$\begin{aligned} J_{\mu\mu} &= 8N|V_\mu(k_\mu)|^2 \left(1 - \left| \sum_k \bar{\psi}_0(k) \psi_0(k-k_\mu) \right|^2 \right) \\ &= 8N|V_\mu(k_\mu)|^2 (1 - |C(k_\mu)|^2), \end{aligned} \quad (\text{SM.23})$$

which is (14) given in the main text. $J_{\mu\mu}$ vanishes for $k_\mu = 0$ (as it does for phase-contrast TEM). If we regard k_μ as nonzero but otherwise arbitrary, then $J_{\mu\mu}$ is maximized by a single plane wave. If we further stipulate a finite aperture size K , then $J_{\mu\mu}$ is near-maximized by ‘‘random’’ aberrations, corresponding to a delocalized speckled probe.

We also supply the following derivation using a coordinate representation. In this space, the derivatives of the potential have the forms

$$V_\mu(x) = \begin{cases} 2 \cos[2\pi k_\mu \cdot x + \phi(k_\mu)] & \text{for } \lambda_\mu = |V(k_\mu)|, \\ 2|V(k_\mu)| \sin[2\pi k_\mu \cdot x + \phi(k_\mu)] & \text{for } \lambda_\mu = \arg V(k_\mu). \end{cases} \quad (\text{SM.24})$$

In light of the above, we can set $\mu = \nu$ at the outset, and obtain

$$\begin{aligned}
J_{\mu\mu} &= \frac{4N}{M} \sum_x \operatorname{Re} \langle \psi_\mu(x) | e^{+i\hat{V}} \hat{V}_\mu (1 - e^{-i\hat{V}} |\psi_0(x)\rangle \langle \psi_0(x) | e^{+i\hat{V}}) \hat{V}_\mu e^{-i\hat{V}} | \psi_0(x) \rangle \\
&= \frac{4N}{M^2} \sum_{x,x'} V_\mu^2(x') |\psi_0(x' - x)|^2 - \frac{4N}{M^3} \sum_x \left(\sum_{x'} V_\mu(x') |\psi_0(x' - x)|^2 \right)^2 \\
&= \frac{4N}{M} \sum_{x'} V_\mu^2(x') - \frac{4N}{M} \sum_x \left(\frac{1}{M} \sum_{x'} V_\mu(x') [|\psi_0(x' - x)|^2 - 1] \right)^2.
\end{aligned} \tag{SM.25}$$

The second summation in the last line is a sum of squares. Therefore, if the spatial frequency k_μ of $V_\mu(x)$ is nonzero but otherwise arbitrary, then $J_{\mu\mu}$ is maximized by a STEM probe whose intensity in coordinate space has minimal correlation with any such $V_\mu(x)$. Apart from a plane wave (which has zero correlation with $V_\mu(x)$ so that the entire summation in question vanishes), for a finite aperture, a delocalized speckled intensity distribution has near-minimal correlation and will near-maximize $J_{\mu\mu}$.

QUANTUM-LIMIT CONDITIONS FOR 4D-STEM

Starting with the conditions (4), we incorporate the beam position, and we appropriately adopt for the PVM the complete set of projectors onto Fourier space $\{|k\rangle\langle k|\}$, to obtain

$$\langle \psi(x) | [\hat{H}_\mu, \hat{H}_\nu] | \psi(x) \rangle = 0 \quad \forall x, k_\mu \text{ and } k_\nu, \tag{SM.26a}$$

$$\langle \psi(x) | k \rangle \langle k | \hat{Q}(x) | \psi_\mu(x) \rangle \in \mathbb{R} \quad \forall x, k \text{ and } k_\mu. \tag{SM.26b}$$

Under the WPOA, $\hat{H}_\mu = \hat{V}_\mu$, so that the commutativity condition (SM.26a) is always satisfied (the same holds under the POA).

Reality condition for the bright field

For a wave vector k in the bright field, the reality condition (SM.26b) becomes, to leading order in \hat{V} ,

$$\begin{aligned}
\langle \psi(x) | k \rangle \langle k | \hat{Q}(x) | \psi_\mu(x) \rangle &= -i \langle \psi_0(x) | k \rangle \langle k | (1 - |\psi_0(x)\rangle \langle \psi_0(x) |) \hat{V}_\mu | \psi_0(x) \rangle \\
&= -i \bar{\psi}_0(k) e^{2\pi i k \cdot x} \sum_{k', k''} [\delta_{k, k'} - \psi_0(k) \bar{\psi}_0(k') e^{-2\pi i (k - k') \cdot x}] V_\mu(k' - k'') \psi_0(k'') e^{-2\pi i k'' \cdot x} \\
&= -i \bar{\psi}_0(k) \psi_0(k - k_\mu) V_\mu(k_\mu) e^{+2\pi i k_\mu \cdot x} + (+k_\mu \rightarrow -k_\mu) \\
&\quad + i |\psi_0(k)|^2 \sum_{k'} \bar{\psi}_0(k') \psi_0(k' - k_\mu) V_\mu(k_\mu) e^{+2\pi i k_\mu \cdot x} + (+k_\mu \rightarrow -k_\mu) \\
&= -i \bar{\psi}_0(k) \psi_0(k - k_\mu) V_\mu(k_\mu) e^{+2\pi i k_\mu \cdot x} + (+k_\mu \rightarrow -k_\mu) \\
&\quad + \frac{i}{M_K} C(k_\mu) V_\mu(k_\mu) e^{+2\pi i k_\mu \cdot x} + (+k_\mu \rightarrow -k_\mu) \in \mathbb{R} \quad \forall x, k \text{ and } k_\mu,
\end{aligned} \tag{SM.27}$$

where $M_K = 1/|\psi_0(k)|^2$ for $|k| \leq K$. M_K is just the number of wave vectors inside the STEM objective aperture. Recall that we must have $|C(k_\mu)|^2 \ll 1$, otherwise the QFIM is significantly diminished compared with phase-contrast TEM. A diminished QFIM in STEM is achieved by using, e.g., a highly defocused probe or, better, a speckled probe, in which case $\langle |C(k_\mu)|^2 \rangle \leq 1/M_K \ll 1$. We assume such a relevant case. Hence, in the last line above, we can neglect the term containing $C(k_\mu)$ to obtain

$$-i \bar{\psi}_0(k) \psi_0(k - k_\mu) V_\mu(k_\mu) e^{+2\pi i k_\mu \cdot x} + (+k_\mu \rightarrow -k_\mu) \in \mathbb{R} \quad \forall x, k \text{ and } k_\mu, \tag{SM.28}$$

which is the bright-field reality condition (15) in the main text.

Reality condition for the dark field

For k in the dark field, to leading order in \hat{V} , the projection operator $\hat{Q}(x)$ can be replaced with the identity, and the condition (SM.26b) becomes

$$\begin{aligned}
\langle \psi(x)|k\rangle\langle k|\hat{Q}(x)|\psi_\mu(x)\rangle &= \langle \psi_0(x)|\hat{V}|k\rangle\langle k|\hat{V}_\mu|\psi_0(x)\rangle \\
&= \sum_{k',k''} \bar{\psi}_0(k')V(k'-k)V_\mu(k-k'')\psi_0(k'')e^{2\pi i(k'-k'')\cdot x} \\
&= \sum_{k'} \bar{\psi}_0(k-k')\bar{V}(k')V_\mu(k_\mu)\psi_0(k-k_\mu)e^{-2\pi i(k'-k_\mu)\cdot x} + (+k_\mu \rightarrow -k_\mu) \in \mathbb{R}
\end{aligned} \tag{SM.29}$$

$\forall x, |k| > K \text{ and } k_\mu,$

which is (16) in the main text.

CALCULATION OF $I_{\mu\nu}$ FOR 4D-STEM

Using the property of additivity, it is straightforward to incorporate the beam position x into the definition of the CFIM I :

$$\begin{aligned}
I_{\mu\nu} &= \frac{N}{M} \sum_{k,x} p(k,x)(\partial_\mu \ln p(k,x))(\partial_\nu \ln p(k,x)) \\
&= \frac{4N}{M} \sum_{k,x} \frac{\text{Re}\{\langle \psi_\mu(x)|k\rangle\langle k|\psi(x)\rangle\}\text{Re}\{\langle \psi(x)|k\rangle\langle k|\psi_\nu(x)\rangle\}}{\langle k|\psi(x)\rangle\langle \psi(x)|k\rangle},
\end{aligned} \tag{SM.30}$$

where $p(k,x) = (1/M)|\langle k|\psi(x)\rangle|^2$.

Bright-field contribution

For the bright-field, we stipulate that k lies inside the (image of the) probe-forming aperture, that is, $|k| \leq K$. In the WPOA, we obtain, to leading order in \hat{V} ,

$$I_{\mu\nu}^{\text{BF}} = \frac{4N}{M} \sum_{|k|\leq K,x} \frac{\text{Re}\{\langle \psi_0(x)|i\hat{V}_\mu|k\rangle\langle k|\psi_0(x)\rangle\}\text{Re}\{\langle \psi_0(x)|k\rangle\langle k|(-i)\hat{V}_\nu|\psi_0(x)\rangle\}}{\langle k|\psi_0(x)\rangle\langle \psi_0(x)|k\rangle}. \tag{SM.31}$$

For the factor containing ν , we obtain

$$\begin{aligned}
\frac{\text{Re}\{\langle \psi_0(x)|k\rangle\langle k|(-i)\hat{V}_\nu|\psi_0(x)\rangle\}}{|\langle \psi_0(x)|k\rangle|} &= |V_\nu(k_\nu)| |\psi_0(k-k_\nu)| \sin[2\pi(\chi(k) - \chi(k-k_\nu)) + 2\pi k_\nu \cdot x + \phi_\nu(k_\nu)] \\
&\quad + |V_\nu(k_\nu)| |\psi_0(k+k_\nu)| \sin[2\pi(\chi(k) - \chi(k+k_\nu)) - 2\pi k_\nu \cdot x - \phi_\nu(k_\nu)].
\end{aligned} \tag{SM.32}$$

A similar result is obtained for the factor containing μ , and so the CFIM consists of four terms “ $+k_\mu, +k_\nu$,” “ $-k_\mu, +k_\nu$,” “ $+k_\mu, -k_\nu$ ” and “ $-k_\mu, -k_\nu$.” Only the sine functions depend on the probe position x , and we can perform the summation over x using the generic expression

$$\frac{1}{M} \sum_x \sin[2\pi a + 2\pi k_\mu \cdot x] \sin[2\pi b + 2\pi k_\nu \cdot x] = \frac{1}{2} \delta_{k_\mu, k_\nu} \cos[2\pi(a-b)] - \frac{1}{2} \delta_{k_\mu, -k_\nu} \cos[2\pi(a+b)]. \tag{SM.33}$$

Using this expression, after some algebra, we obtain a non-zero result only for the diagonal terms

$$I_{\mu\mu}^{\text{BF}} = 4N|V_\mu(k_\mu)|^2 \sum_{|k|\leq K} (|\psi_0(k-k_\mu)|^2 - |\psi_0(k-k_\mu)||\psi_0(k+k_\mu)| \cos[2\pi(2\chi(k) - \chi(k-k_\mu) - \chi(k+k_\mu))]). \tag{SM.34}$$

Dark-field contribution

For the dark field, k lies outside of the (image of the) probe-forming aperture, that is, $|k| > K$. To leading order in \hat{V} , we obtain

$$I_{\mu\nu}^{\text{DF}} = \frac{4N}{M} \sum_{|k|>K,x} \frac{\text{Re}\{\langle\psi_0(x)|\hat{V}_\mu|k\rangle\langle k|\hat{V}|\psi_0(x)\rangle\}\text{Re}\{\langle\psi_0(x)|\hat{V}|k\rangle\langle k|\hat{V}_\nu|\psi_0(x)\rangle\}}{\langle k|\hat{V}|\psi_0(x)\rangle\langle\psi_0(x)|\hat{V}|k\rangle}. \quad (\text{SM.35})$$

The factor $|\langle k|\hat{V}|\psi_0(x)\rangle|^2$ in the denominator cancels with the factors in the numerator, so that this expression is second order in \hat{V} just like the bright field contribution. Writing each of the matrix elements $\langle a|b|c\rangle$ in the above expression in terms of its modulus $|\langle a|b|c\rangle|$ and phase $\arg\langle a|b|c\rangle$, we can obtain after some algebra

$$I_{\mu\nu}^{\text{DF}} = \frac{2N|V_\mu(k_\mu)||V_\nu(k_\nu)|}{M} \sum_{|k|>K,x} |\psi_0(k-k_\mu)||\psi_0(k-k_\nu)|(\delta_{\mu\nu} + \cos[\varphi_\mu(k,x) + \varphi_\nu(k,x) - 2\varphi(k,x)]) \\ + (+k_\mu \rightarrow -k_\mu, +k_\nu \rightarrow -k_\nu), \quad (\text{SM.36})$$

where

$$\varphi_\mu(k,x) = \arg\langle k|\hat{V}_\mu|\psi_0(x)\rangle + 2\pi k \cdot x = 2\pi k_\mu \cdot x - 2\pi\chi(k-k_\mu) + \phi_\mu(k_\mu), \quad (\text{SM.37})$$

with an analogous expression for $\arg_\nu(k,x)$, and

$$\varphi(k,x) = \arg\langle k|\hat{V}|\psi_0(x)\rangle + 2\pi k \cdot x = \arg \sum_{k'} V(k')\psi_0(k-k')e^{+2\pi i k' \cdot x}. \quad (\text{SM.38})$$

Expression (SM.36) contains two parts, one featuring $+k_\mu, +k_\nu$ (as written out explicitly) and the other featuring $-k_\mu, -k_\nu$ (as indicated by the shorthand notation). For a given k , only one of those parts can be nonzero, but the summation over k means that both parts always contribute. Notice that the presence of the cosine terms means that $I_{\mu\nu}^{\text{DF}}$ is *not* diagonal. Also notice that $\varphi(k,x)$ depends explicitly on the values of the Fourier coefficients participating in the summation over k' , which makes further simplifications of (SM.36) difficult. However, as we will see below, the generic behavior is that the cosine terms tend to cancel out. And if we make the approximation to omit the cosine terms entirely, then $I_{\mu\nu}^{\text{DF}}$ is diagonal, with the diagonal elements taking the very simple form

$$I_{\mu\mu}^{\text{DF}} \approx 4N|V_\mu(k_\mu)|^2 \sum_{|k|>K} |\psi_0(k-k_\mu)|^2. \quad (\text{SM.39})$$

Consider a diagonal element of (SM.36), that is, set $\mu = \nu$, and consider the case of aberrations χ that are random on $[0, 2\pi)$. In $\varphi(k,x)$, the summation over k' will execute a *random walk* in the Argand plane, producing an expected phase which is random on $[0, 2\pi)$ (and an expected magnitude $\sqrt{\sum_{k'} |\psi_0(k-k')||\bar{V}(k')|}$ which has cancelled out). Hence $\varphi(k,x)$ inside the cosine in (SM.36) is just a random phase. However, the presence of $\varphi_\mu(k,x)$ means that the phase of the term $k' = k_\mu$ is not random, which results in a *biased* random walk. The degree of bias is determined by the size of $|V(k_\mu)|$ relative to the moduli of the other Fourier coefficients participating in the summation over k' . If $|V(k_\mu)|$ dominates the summation, as it can when the STEM objective aperture is small enough that the diffracted discs do not overlap significantly, then the random walk is not random at all, and we obtain for the argument of the cosine

$$2\varphi_\mu(k,x) - 2\varphi(k,x) \approx 2\phi_\mu(k_\mu) - 2\phi(k_\mu) = \begin{cases} 0 & \text{for } \lambda_\mu = |V(k_\mu)|, \\ \pi & \text{for } \lambda_\mu = \arg V(k_\mu). \end{cases} \quad (\text{SM.40})$$

Substituting into the expression for $I_{\mu\nu}^{\text{DF}}$, we obtain

$$I_{\mu\mu}^{\text{DF}} \approx \begin{cases} 8N \sum_{|k|>K} |\psi_0(k-k_\mu)|^2 & \text{for } \lambda_\mu = |V(k_\mu)|, \\ 0 & \text{for } \lambda_\mu = \arg V(k_\mu). \end{cases} \quad (\text{SM.41})$$

In this case, we have obtained approximately full modulus information but no phase information (as expected, because this is just the classic “phase problem” of parallel-beam diffraction). On the other hand, if $|V(k_\mu)|$ does not dominate,

as is the case when the STEM objective aperture is large and multiple diffracted discs overlap significantly, then the argument of each cosine is effectively random on $[0, 2\pi)$, and the cosines will tend to cancel out. In this case, we obtain

$$I_{\mu\mu}^{\text{DF}} \approx \begin{cases} 4N \sum_{|k|>K} |\psi_0(k - k_\mu)|^2 & \text{for } \lambda_\mu = |V(k_\mu)|, \\ 4N |V(k_\mu)|^2 \sum_{|k|>K} |\psi_0(k - k_\mu)|^2 & \text{for } \lambda_\mu = \arg V(k_\mu). \end{cases} \quad (\text{SM.42})$$

In this case, we have obtained approximately half of the modulus information and half of the phase information. We regard the latter case as the “generic case” for 4D-STEM.

Now, still considering a diagonal element, consider the focused case $\chi = 0$ (the other extreme). In this case, the phase factors involving x , while not random, will, when averaged over x , produce results very similar to those above. That is, when $|V(k_\mu)|$ dominates we obtain approximately full modulus information but no phase information, and when $|V(k_\mu)|$ does not dominate (the generic case) we obtain approximately half of the modulus information and half of the phase information.

The above findings are supported by the following table which shows numerical calculations of $I_{\mu\mu}^{\text{DF}}$ for three different materials and three different aberration conditions (those described in the main text). The table assumes a 100 keV beam with a 20 mrad convergence semi-angle ($K = 0.54 \text{ \AA}^{-1}$). The defocused cases use $C_1 = -100 \text{ nm}$. The right-hand side of the table shows the values obtained for $I_{\mu\mu}^{\text{DF}}$ (normalized such that a value of unity means full information). Most values are close to 0.5, i.e., half of the information. Strong reflections tend to give more modulus information than phase information. The values exhibit only a weak dependence on the aberrations. These behaviors persist for higher-order reflections (not shown). COF is an acronym for covalent organic framework.

Sample	k_μ	d (Å)	$V(k_\mu)$ (eV)		Focused		Defocused		Speckled	
			Re	Im	mod	arg	mod	arg	mod	arg
SrTiO ₃ [001]	(1, 0, 0)	3.91	+0.02	0.0	0.47	0.53	0.50	0.50	0.50	0.50
	(1, 1, 0)	2.76	+6.05	0.0	0.55	0.45	0.54	0.46	0.55	0.45
	(2, 0, 0)	1.95	+7.89	0.0	0.63	0.37	0.62	0.38	0.62	0.38
	(2, 1, 0)	1.75	-0.15	0.0	0.52	0.48	0.46	0.54	0.50	0.50
	(2, 2, 0)	1.38	+5.22	0.0	0.60	0.40	0.58	0.42	0.59	0.41
Graphene	(1, 0, 0)	2.13	+1.66	-2.88	0.59	0.41	0.59	0.41	0.59	0.41
	(1, 1, 0)	1.23	+2.96	0.0	0.71	0.29	0.70	0.30	0.71	0.29
	(2, 0, 0)	1.07	+0.56	+0.97	0.63	0.37	0.62	0.38	0.61	0.39
COF-1 [001]	(6, $\bar{3}$, 0)	2.61	-0.14	0.0	0.57	0.43	0.52	0.48	0.50	0.50
	(6, 0, 0)	2.26	-0.69	0.0	0.55	0.45	0.55	0.45	0.55	0.45
	(12, $\bar{6}$, 0)	1.30	+0.63	0.0	0.61	0.39	0.59	0.41	0.59	0.41
	(12, 0, 0)	1.13	-0.22	0.0	0.52	0.48	0.52	0.48	0.52	0.48

The following table includes both diagonal and off-diagonal elements of $I_{\mu\nu}^{\text{DF}}$ for the case of a focused probe on SrTiO₃ [001]. $I_{\mu\nu}^{\text{DF}}$ is a real-symmetric matrix so that values below the diagonal have been omitted. The largest off-diagonal (in terms of magnitude) is about 5 times smaller than a typical diagonal, and most off-diagonals are considerably smaller still. Note the symmetries: (1) diagonal mod-arg pairs sum to unity, (2) off-diagonal mod-arg pairs sum to zero, and (3) all mixed mod-arg elements are zero. These symmetries can be inferred from (SM.36).

SrTiO ₃ [001]	(1, 0, 0)		(1, 1, 0)		(2, 0, 0)		(2, 1, 0)		(2, 2, 0)		
	mod	arg	mod	arg	mod	arg	mod	arg	mod	arg	
(1, 0, 0)	mod	0.47	0	0.003	0	0.001	0	-0.06	0	-0.0004	0
	arg		0.53	0	-0.003	0	-0.0009	0	0.06	0	0.0004
(1, 1, 0)	mod		0.55	0	0.08	0	0.001	0	0.04	0	
	arg			0.45	0	-0.08	0	-0.001	0	-0.04	
(2, 0, 0)	mod				0.63	0	0.002	0	0.05	0	
	arg					0.37	0	-0.002	0	-0.05	
(2, 1, 0)	mod						0.52	0	0.001	0	
	arg							0.48	0	-0.001	
(2, 2, 0)	mod								0.60	0	
	arg									0.40	

Complete bright- and dark-field contribution

Adding the generic dark-field component (when $|V(k_\mu)|$ does not dominate) to the bright-field component calculated earlier, we obtain the (approximate) complete CFIM for STEM (under the WPOA)

$$I_{\mu\mu} \approx 4N|V_\mu(k_\mu)|^2 \left(1 - \sum_k |\psi_0(k - k_\mu)| |\psi_0(k + k_\mu)| \cos[2\pi(2\chi(k) - \chi(k - k_\mu) - \chi(k + k_\mu))] \right), \quad (\text{SM.43})$$

which is (17) stated in the main text.
